

A bistatic CCD receiver model for airborne lidar returns from underwater objects

Nail Çadalli, David C. Munson, Jr. and Andrew C. Singer

Coordinated Science Laboratory

University of Illinois at Urbana-Champaign,

1308 West Main Street, Urbana, IL 61801, U. S. A.

{cadalli, d-munson, singer}@ifp.uiuc.edu

We describe a model for airborne lidar returns collected by a charge-coupled device (CCD) receiver from underwater objects together with returns from the water medium and ocean bottom. The model exploits bistatic lidar equations to obtain the return at each element of the CCD array. The lidar equations account for multiple scattering and absorption in the water column illuminated from an airborne lidar. A comparison of simulated CCD outputs with real ocean lidar data is included. © 2001 Optical Society of America

OCIS codes: 010.3640 Lidar, 030.5620 Radiative transfer, 040.1520 CCD charge-coupled device, 110.4100 Modulation transfer function, 290.4210 Multiple scattering, 999.9999 bistatic lidar equations, 010.3310 Laser beam transmission, 010.4450 Ocean optics, 290.1350 Backscattering.

1. Introduction

One of the applications of pulsed lidar systems is airborne imaging for detection, localization and classification of underwater objects. An airborne lidar system typically uses a CCD camera to

determine the shape of an object in the water column illuminated by the broad laser beam. In addition, the system may use a photomultiplier tube (PMT) to obtain the depth of the object. A PMT provides a highly time-resolved photoelectron count as a function of time from the lidar return, which in turn can provide accurate depth information. On the other hand, a CCD array provides a pixelized image of the field of view. The output of each CCD element, corresponding to a pixel in the image, is the sum of light radiance in the time interval over which the CCD is gated. Such gating, or integration time, is necessary to build up sufficient signal power, since the CCD array divides the total return into a large number of pixels.

This paper presents a model for airborne lidar returns received at a CCD array. We develop lidar equations for a bistatic geometry where the transmitter and receiver can be at different locations looking in different directions. The bistatic lidar equations are the generalized form of monostatic (or collinear) lidar equations, where the receiver is boresighted to the transmitter and is positioned at the same location with the transmitter (or at a different location that is along the line of sight). While the monostatic lidar equations are suitable for simulation of PMT returns, the bistatic lidar equations are needed for simulation of CCD returns. We treat each CCD element as a separate receiver with appropriate position and direction offsets, and use the bistatic lidar equations to compute the corresponding return.

The monostatic lidar model on which we have based our development is from Walker, McLean et al.¹⁻³ This lidar model exploits the small-angle scattering approximation, and takes into account multiple scattering with time dispersion. The model provides analytical expressions for the lidar returns based on a statistical model for the beam spread function. These expressions have been reported to be in agreement with multiple-scattering Monte-Carlo simulations and real lidar data.

We first present the bistatic lidar equations and then describe the details of the application of these equations to CCD modeling and simulation. We then show an example simulated lidar return

that is computed using these equations, and we present a CCD image from a real ocean data set for comparison.

2. Bistatic lidar equations

The theory that describes the propagation of electromagnetic energy in highly scattering media such as ocean waters is called *radiative transport theory*.^{4–10} The radiative transport equation, which is the counterpart of Maxwell’s equations, can be derived using the conservation of energy principle. Via small-angle scattering approximations, the radiative transport equation can be solved by Fourier transform methods. For oceanic hydrosols, particle dimensions are large compared to the wavelength, and light scattered by such particles is confined to small angles about the ray axis. The derivation of bistatic lidar equations to be presented in this section makes extensive use of radiative transport theory and the small-angle scattering approximation. The derivation is similar to, but more general than, that of the monostatic lidar equations given by Walker and McLean.¹ For consistency and to facilitate comparison with their results, we use similar nomenclature to theirs.

Let the light radiance at a particular point in space, in a specific direction and at a particular time instant, be denoted by $L(z, \boldsymbol{\rho}, \boldsymbol{s}, t)$. Here, the position vector is $\hat{\boldsymbol{i}}x + \hat{\boldsymbol{j}}y + \hat{\boldsymbol{k}}z = \boldsymbol{\rho} + \hat{\boldsymbol{k}}z$, the direction vector is $\hat{\boldsymbol{s}} = \hat{\boldsymbol{i}} \sin \theta \cos \phi + \hat{\boldsymbol{j}} \sin \theta \sin \phi + \hat{\boldsymbol{k}} \cos \theta$, and t represents the time. The boldface characters represent vectors. A unit vector is indicated by a hat. The small-angle scattering assumption yields $\sin \theta \approx \theta$ and $\cos \theta \approx 1$ for small θ . Then, the direction vector can be approximated as $\hat{\boldsymbol{s}} \approx \boldsymbol{s} + \hat{\boldsymbol{k}}$, where $\boldsymbol{s} = \hat{\boldsymbol{i}}\theta \cos \phi + \hat{\boldsymbol{j}}\theta \sin \phi$. The small-angle scattering assumption dictates the so-called forward scattering regime, where $s = |\boldsymbol{s}| \ll 1$ and $\rho = |\boldsymbol{\rho}| \ll z$.

Let the radiance for a laser source with pulse energy Q , located at the origin and looking in the z direction, be $L(0, \boldsymbol{\rho}, \boldsymbol{s}, t) = Q \delta(\boldsymbol{\rho}) \delta(\boldsymbol{s}) \delta(t)$. Note that, the pulse is modeled by an

impulse. To incorporate the pulse shape, we convolve the lidar return, calculated later in this paper, with the laser pulse. The radiance after propagating a distance z to the target plane is $L(z, \boldsymbol{\rho}, \mathbf{s}, t) = Q k(z, \boldsymbol{\rho}, \mathbf{s}, \tau)$, where the *medium beam spread function* is denoted by $k(z, \boldsymbol{\rho}, \mathbf{s}, \tau)$. The beam spread function is the impulse response of the medium, and it can be used (as a Green's function) to obtain the total response of the medium to an arbitrary source. The *multipath time* is given by $\tau = t - z/c$, where c is the speed of light in the medium through which the light travels. The multipath time is the amount of excess time required for a scattered photon to arrive at the target plane. The *medium transfer function* $K(z, \boldsymbol{\kappa}, \mathbf{q}, \tau)$ is the Fourier transform of the beam spread function.^{1,10} The vectors $\boldsymbol{\kappa}$ and \mathbf{q} represent the spatial and angular frequency variables corresponding to $\boldsymbol{\rho}$ and \mathbf{s} , respectively.

For a source at $\boldsymbol{\rho}'$ and with beam axis in the direction $\hat{\mathbf{s}}' = \mathbf{s}' + \hat{\mathbf{k}}$, we have

$$L(0, \boldsymbol{\rho}, \mathbf{s}, t) = Q \delta(\boldsymbol{\rho} - \boldsymbol{\rho}') \delta(\mathbf{s} - \mathbf{s}') \delta(t) . \quad (1)$$

Here $s' = |\mathbf{s}'| = \theta \ll 1$, i.e. the radiation direction (the angle between the beam axis and the z axis) is small. The beam axis offset is, therefore, given by $\boldsymbol{\rho}' + z\mathbf{s}'$. The radiance at the target plane is given as,^{1,11}

$$L(z, \boldsymbol{\rho}, \mathbf{s}, t) = Q k(z, \boldsymbol{\rho} - (\boldsymbol{\rho}' + z\mathbf{s}'), \mathbf{s} - \mathbf{s}', \tau) . \quad (2)$$

and the radiance in the target plane due to a shaped laser beam is

$$L(z, \boldsymbol{\rho}, \mathbf{s}, t) = Q \int \dots \int \psi(\boldsymbol{\rho}') \theta(\mathbf{s}') k(z, \boldsymbol{\rho} - (\boldsymbol{\rho}' + z\mathbf{s}'), \mathbf{s} - \mathbf{s}', \tau) d\boldsymbol{\rho}' ds', \quad (3)$$

where the beam spread function $k(z, \boldsymbol{\rho}, \mathbf{s}, \tau)$ is convolved with the *aperture function* $\psi(\boldsymbol{\rho})$ that specifies the spatial extent of the source and with the function $\theta(\mathbf{s})$ that specifies the (*angular radiation pattern*) of the source. Inserting the inverse Fourier transform expression, containing the medium transfer function, in place of the beam spread function, we have

$$L(z, \boldsymbol{\rho}, \mathbf{s}, t) = \frac{Q}{(2\pi)^4} \int \dots \int \Psi(\boldsymbol{\kappa}) \Theta(\mathbf{q} + \boldsymbol{\kappa}z) K(z, \boldsymbol{\kappa}, \mathbf{q}, \tau) \exp(-j(\boldsymbol{\kappa} \cdot \boldsymbol{\rho} + \mathbf{q} \cdot \mathbf{s})) d\boldsymbol{\kappa} d\mathbf{q}. \quad (4)$$

Consider now a transmitter (laser source) that has position and direction offsets $\boldsymbol{\rho}_{TX}$ and \boldsymbol{s}_{TX} , respectively. The offset functions are $\psi_{TX}(\boldsymbol{\rho} - \boldsymbol{\rho}_{TX})$ and $\theta_{TX}(\boldsymbol{s} - \boldsymbol{s}_{TX})$ with Fourier transforms $\Psi_{TX}(\boldsymbol{\kappa}) \exp(j\boldsymbol{\kappa} \cdot \boldsymbol{\rho}_{TX})$ and $\Theta_{TX}(\boldsymbol{q}) \exp(j\boldsymbol{q} \cdot \boldsymbol{s}_{TX})$, respectively. Thus, we have

$$L(z, \boldsymbol{\rho}, \boldsymbol{s}, t) = \frac{Q}{(2\pi)^4} \int \cdots \int \Psi_{TX}(\boldsymbol{\kappa}) \Theta_{TX}(\boldsymbol{q} + \boldsymbol{\kappa}z) K(z, \boldsymbol{\kappa}, \boldsymbol{q}, \tau) \cdot \exp(j\boldsymbol{\kappa} \cdot \boldsymbol{\rho}_{TX}) \exp(j(\boldsymbol{q} + \boldsymbol{\kappa}z) \cdot \boldsymbol{s}_{TX}) \exp(-j(\boldsymbol{\kappa} \cdot \boldsymbol{\rho} + \boldsymbol{q} \cdot \boldsymbol{s})) d\boldsymbol{\kappa} d\boldsymbol{q} \quad (5)$$

as the radiance at the target plane due to an offset transmitter.

Consider the airborne lidar geometry depicted in Figure 1, where TX and RX denote a transmitter (laser source) and a receiver (CCD element). The transmitter and the receiver are, in general, at different locations and pointed in different directions. This is a *bistatic* geometry. The geometry where the transmitter and receiver are at the same location and have the same directional orientation is called a *monostatic* geometry. To handle the bistatic case, we assign position offset $\boldsymbol{\rho}_{RX}$, to the aperture function, $\psi_{RX}(\boldsymbol{\rho})$, of the receiver and direction offset \boldsymbol{s}_{RX} to the receiver pattern, $\theta_{RX}(\boldsymbol{s})$. The altitude of the transmitter and receiver from the water surface is H .

A. Bottom return

The method of computation of the bottom return provides insight and a basis for the computation of the lidar return from the water medium and an underwater object. We first calculate the radiance incident on the bottom of the water column, which is usually the ocean bottom in, for instance, shallow-water mine imaging. Let the bottom be at depth $z = D$ in Figure 1. We incorporate refraction at the air-water interface. Let m denote the index of refraction for water, which is approximately equal to $4/3$.⁹ The index of refraction for air is assumed to be unity. Then, denoting the speed of light in air by c , we have c/m as the speed of light in water. We assume that the atmosphere is dispersionless with transmission coefficient T_a . The transmission coefficient for the air-water interface is given by $T_{aw} = (\frac{1-m}{1+m})^2$, since water does not display any significant magnetic

properties, and hence the permeability of water is close to that of air. Applying Snell's law at the air-water interface in Figure 1, we have $\sin \theta_1 = m \sin \theta_2$. Due to the small-angle assumption, this becomes $\theta_1 = m \theta_2$. Then, the position offset of the transmitter associated with the downwelling path is

$$z \tan \theta_2 + H \tan \theta_1 \approx z \theta_2 + H \theta_1 = (z + Hm) \theta_2 . \quad (6)$$

Note that in (3), $\boldsymbol{\rho}'$ and \boldsymbol{s}' denote the offset position and direction in the water. Here, \boldsymbol{s}' stands for the direction offset of the airborne transmitter, and hence the corresponding angle in water is \boldsymbol{s}'/m due to refraction. Using these modifications in (5) in order to incorporate the air-water interface and the resulting refraction, we have the following expression for the transmitted radiance incident on the bottom:

$$\begin{aligned} L_{TX}(H + z, \boldsymbol{\rho}, \boldsymbol{s}, t) &= \frac{QT_a T_{aw}}{(2\pi)^4} \int \dots \int \Psi_{TX}(\boldsymbol{\kappa}) \Theta_{TX}(\mathbf{q}/m + \boldsymbol{\kappa}(H + z/m)) K(z, \boldsymbol{\kappa}, \mathbf{q}, \tau) \\ &\cdot \exp(j\boldsymbol{\kappa} \cdot \boldsymbol{\rho}_{TX}) \exp(j(\mathbf{q}/m + \boldsymbol{\kappa}(H + z/m)) \cdot \boldsymbol{s}_{TX}) \exp(-j(\boldsymbol{\kappa} \cdot \boldsymbol{\rho} + \mathbf{q} \cdot \boldsymbol{s})) d\boldsymbol{\kappa} d\mathbf{q}, \quad (7) \end{aligned}$$

where $t = H/c + zm/c + \tau$. The reflected radiance from the bottom is given by

$$\begin{aligned} L_{back}(H + z, \boldsymbol{\rho}, \boldsymbol{s}, t) &= \frac{R}{\pi} \iint L_{TX}(H + z, \boldsymbol{\rho}, \boldsymbol{s}, t) d\boldsymbol{s} \\ &= \frac{Q T_a T_{aw} R}{\pi(2\pi)^2} \iint \Psi_{TX}(\boldsymbol{\kappa}) \Theta_{TX}(\boldsymbol{\kappa}(H + z/m)) K(z, \boldsymbol{\kappa}, \mathbf{0}, \tau) \\ &\cdot \exp(j\boldsymbol{\kappa} \cdot (\boldsymbol{\rho}_{TX} + (H + z/m)\boldsymbol{s}_{TX})) \exp(-j\boldsymbol{\kappa} \cdot \boldsymbol{\rho}) d\boldsymbol{\kappa} d\mathbf{q}, \quad (8) \end{aligned}$$

where R is the bottom reflectance. Notice that the integral over \boldsymbol{s} is the irradiance, which is the sum of the radiance from all directions, associated with a particular point on the bottom. To find the radiance presented to the receiver, we assume that each point on the bottom is a diffuse source. The radiance incident on the receiver is then a convolution over $\boldsymbol{\rho}$ and t between the reflected irradiance L_{back} and the radiance due to a diffuse source. For a diffuse source, the radiance in the

target plane at a distance z in the direction $\hat{\mathbf{s}} \approx \mathbf{s} + \hat{\mathbf{k}}$ is given by

$$L_{dif}(z, \boldsymbol{\rho}, \mathbf{s}, t) = \frac{1}{(2\pi)^2} \iint K(z, \boldsymbol{\kappa}, -z\boldsymbol{\kappa}, \tau) \exp(-j\boldsymbol{\kappa} \cdot (\boldsymbol{\rho} - z\mathbf{s})) d\boldsymbol{\kappa}. \quad (9)$$

According to our coordinate convention in Figure 1, the vector \mathbf{s} in (7) represents the direction $\hat{\mathbf{s}} \approx \mathbf{s} + \hat{\mathbf{k}}$, with $\hat{\mathbf{k}}$ being downward. Thus, in expressing L_{dif} , we need to use $-\hat{\mathbf{s}}$ in order to take into account the direction of propagation, which is upward from a diffuse source at the bottom towards the airborne receiver. This argument can be justified by the optical reciprocity principle.^{3,9} Hence, for a diffuse source at the bottom radiating upwards (upwelling radiance), we have at the receiver

$$L_{dif}(H + z, \boldsymbol{\rho}, \mathbf{s}, t) = \frac{1}{(2\pi)^2} \iint K(z, \boldsymbol{\kappa}, -z\boldsymbol{\kappa}, \tau) \exp(-j\boldsymbol{\kappa} \cdot (\boldsymbol{\rho} + (H + z/m)\mathbf{s})) d\boldsymbol{\kappa}. \quad (10)$$

Then, the radiance presented to the receiver at an altitude H from the air-water interface is

$$L_{RX}(\boldsymbol{\rho}, \mathbf{s}, t) = \frac{T_a T_{aw}}{m^2} L_{back}(H + z, \boldsymbol{\rho}, \mathbf{s}, t) *_{\boldsymbol{\rho}} *_{\tau} L_{dif}(H + z, \boldsymbol{\rho}, \mathbf{s}, t), \quad (11)$$

where the term $1/m^2$ is due to the Snell cone. The notation $*_{\boldsymbol{\rho}}$ and $*_{\tau}$ denote convolution in the variables $\boldsymbol{\rho}$ and τ . We calculate (11) as

$$\begin{aligned} L_{RX}(\boldsymbol{\rho}, \mathbf{s}, t) &= \frac{Q T_a^2 T_{aw}^2 R}{m^2 \pi (2\pi)^2} \iint \Psi_{TX}(\boldsymbol{\kappa}) \Theta_{TX}(\boldsymbol{\kappa}(H + z/m)) (K(z, \boldsymbol{\kappa}, \mathbf{0}, \tau) *_{\tau} K(z, \boldsymbol{\kappa}, -z\boldsymbol{\kappa}, \tau)) \\ &\quad \cdot \exp(-j\boldsymbol{\kappa} \cdot \boldsymbol{\rho}) \exp(j\boldsymbol{\kappa} \cdot (\boldsymbol{\rho}_{TX} + (H + z/m)\mathbf{s}_{TX})) \exp(-j(H + z/m)\boldsymbol{\kappa} \cdot \mathbf{s}) d\boldsymbol{\kappa} \end{aligned} \quad (12)$$

with $t = 2H/c + 2zm/c + \tau$. To complete the bottom return, we include the receiver field of view (FOV) Ω_{RX} and the receiver aperture area A_{RX} , giving

$$P_b(t) = A_{RX} \Omega_{RX} \int \cdots \int L_{RX}(\boldsymbol{\rho}, \mathbf{s}, t) \psi'_{RX}(\boldsymbol{\rho}) \theta'_{RX}(\mathbf{s}) d\boldsymbol{\rho} d\mathbf{s}, \quad (13)$$

where

$$\begin{aligned} \psi'_{RX}(\boldsymbol{\rho}) &= \psi_{RX}(\boldsymbol{\rho} - \boldsymbol{\rho}_{RX}) \\ \theta'_{RX}(\mathbf{s}) &= \theta_{RX}(\mathbf{s} - \mathbf{s}_{RX}) \end{aligned} \quad (14)$$

are the offset functions specifying the spatial extent and reception pattern of the receiver. Inserting L_{RX} from above and performing the integration over $\boldsymbol{\rho}$ and \boldsymbol{s} using $\Psi'_{RX}(\boldsymbol{\kappa}) = \Psi_{RX}(\boldsymbol{\kappa}) \exp(j\boldsymbol{\kappa} \cdot \boldsymbol{\rho}_{RX})$ and $\Theta'_{RX}(\boldsymbol{q}) = \Theta_{RX}(\boldsymbol{q}) \exp(j\boldsymbol{q} \cdot \boldsymbol{s}_{RX})$ from (14), and noticing that $\psi'_{RX}(\boldsymbol{\rho})$ and $\theta'_{RX}(\boldsymbol{s})$ are real, and hence $\Psi'_{RX}(-\boldsymbol{\kappa}) = (\Psi'_{RX}(\boldsymbol{\kappa}))^*$ and $\Theta'_{RX}(-\boldsymbol{q}) = (\Theta'_{RX}(\boldsymbol{q}))^*$, we have

$$\begin{aligned}
P_b(t) &= \frac{C_b}{(2\pi)^2} \iint \Psi_{TX}(\boldsymbol{\kappa}) \Theta_{TX}(\boldsymbol{\kappa}(H + z/m)) \Psi_{RX}^*(\boldsymbol{\kappa}) \Theta_{RX}^*(\boldsymbol{\kappa}(H + z/m)) \\
&\quad \cdot (K(z, \boldsymbol{\kappa}, \mathbf{0}, \tau) *_\tau K(z, \boldsymbol{\kappa}, -z\boldsymbol{\kappa}, \tau)) \\
&\quad \cdot \exp(j\boldsymbol{\kappa} \cdot ((\boldsymbol{\rho}_{TX} - \boldsymbol{\rho}_{RX}) + (H + z/m)(\boldsymbol{s}_{TX} - \boldsymbol{s}_{RX}))) d\boldsymbol{\kappa}, \tag{15}
\end{aligned}$$

where $t = 2H/c + 2zm/c + \tau$ and $C_b = QA_{RX}\Omega_{RX}T_a^2T_{aw}^2R/(m^2\pi)$. Note that if $\psi_{RX}(\boldsymbol{\rho})$ and $\theta_{RX}(\boldsymbol{s})$ are even functions, the conjugations above can be dropped. For the monostatic case, $\boldsymbol{\rho}_{TX} = \boldsymbol{\rho}_{RX}$ and $\boldsymbol{s}_{TX} = \boldsymbol{s}_{RX}$. If we express the bottom return in terms of the lidar range ζ , we have

$$\begin{aligned}
P_b(\zeta) &= \frac{C_b}{(2\pi)^2} \iint \Psi_{TX}(\boldsymbol{\kappa}) \Theta_{TX}(\boldsymbol{\kappa}(H + D/m)) \Psi_{RX}^*(\boldsymbol{\kappa}) \Theta_{RX}^*(\boldsymbol{\kappa}(H + D/m)) \\
&\quad \cdot (K(D, \boldsymbol{\kappa}, \mathbf{0}, \tau) *_\tau K(D, \boldsymbol{\kappa}, -D\boldsymbol{\kappa}, \tau)) \\
&\quad \cdot \exp(j\boldsymbol{\kappa} \cdot ((\boldsymbol{\rho}_{TX} - \boldsymbol{\rho}_{RX}) + (H + D/m)(\boldsymbol{s}_{TX} - \boldsymbol{s}_{RX}))) d\boldsymbol{\kappa}, \tag{16}
\end{aligned}$$

where $\zeta = D + \frac{c\tau}{2m}$ with D being the bottom depth. Equation (16) is valid for $\zeta \geq D$, that is, after the laser pulse has hit the bottom.

B. Water return

The lidar return from the water medium itself is calculated in a similar manner to the bottom return. Consider the water column as a stack of infinitesimally small layers of water. Then, the backscattered radiance from each interface can be obtained using the bottom return calculation. In this case, the reflectance coefficient R/π is replaced with $\beta(\pi)dz$, and an integration is performed over the lidar range as we keep $t = \tau + 2H/c + 2zm/c$ constant. This accounts for the photons received at a certain time from different layers of water. The term $\beta(\pi)$ is the *volume scattering function* evaluated at

the angle π corresponding to the backward direction. This method of calculation assumes that the backscattered radiation is uniform over a conic section of the backward hemisphere, corresponding to a small-angle cone, with $\beta(\pi) \approx b_b/(2\pi)$ where b_b is the *backscattering coefficient*. We have,

$$\begin{aligned}
P_w(t) &= \frac{C_w}{(2\pi)^2} \int_0^{\frac{c}{2m}(t-2H/c)} \iint \Psi_{TX}(\boldsymbol{\kappa}) \Theta_{TX}(\boldsymbol{\kappa}(H+z/m)) \\
&\cdot \Psi_{RX}^*(\boldsymbol{\kappa}) \Theta_{RX}^*(\boldsymbol{\kappa}(H+z/m)) \exp(j\boldsymbol{\kappa} \cdot ((\boldsymbol{\rho}_{TX} - \boldsymbol{\rho}_{RX}) + (H+z/m)(\mathbf{s}_{TX} - \mathbf{s}_{RX}))) \\
&\cdot (K(z, \boldsymbol{\kappa}, \mathbf{0}, \tau) *_\tau K(z, \boldsymbol{\kappa}, -z\boldsymbol{\kappa}, \tau)) d\boldsymbol{\kappa} dz, \tag{17}
\end{aligned}$$

where $C_w = QA_{RX}\Omega_{RX}T_a^2T_{aw}^2\beta(\pi)/m^2$. Assume $\tau \ll 2zm/c$. With $dz = -\frac{c/m}{2}d\tau$, for the back-ground water return in terms of the lidar range, we have

$$\begin{aligned}
P_w(\zeta) &= \frac{C_w}{(2\pi)^2} \iint \Psi_{TX}(\boldsymbol{\kappa}) \Theta_{TX}(\boldsymbol{\kappa}(H+\zeta/m)) \Psi_{RX}^*(\boldsymbol{\kappa}) \Theta_{RX}^*(\boldsymbol{\kappa}(H+\zeta/m)) \\
&\cdot \exp(j\boldsymbol{\kappa} \cdot ((\boldsymbol{\rho}_{TX} - \boldsymbol{\rho}_{RX}) + (H+\zeta/m)(\mathbf{s}_{TX} - \mathbf{s}_{RX}))) \\
&\cdot \frac{c}{2m} \int_{L_1}^{L_2} (K(\zeta, \boldsymbol{\kappa}, \mathbf{0}, \tau) *_\tau K(\zeta, \boldsymbol{\kappa}, -\zeta\boldsymbol{\kappa}, \tau)) d\tau d\boldsymbol{\kappa}. \tag{18}
\end{aligned}$$

Here, $L_1 = 0$, $L_2 = 2\zeta m/c$ for $\zeta < D$ and $L_1 = 2(\zeta - D)m/c$, $L_2 = 2\zeta m/c$ for $\zeta \geq D$, where D is the bottom depth.

C. Target return

The calculation of the target return and the loss of radiance due to the associated shadow behind the target is similar to the calculation of the bottom and water return, respectively. The radiance backscattered from a flat diffuse target at depth z and location $\boldsymbol{\rho}_t$ is

$$L_{back} = A_t \frac{R_t}{\pi} \delta(\boldsymbol{\rho} - \boldsymbol{\rho}_t) \iint L_{TX}(H+z, \boldsymbol{\rho}, \mathbf{s}, t) d\mathbf{s}, \tag{19}$$

where A_t is the area of the reflecting surface, R_t is the reflectance of the target, and L_{TX} is as given in (7). Inserting (7) into (19) yields

$$\begin{aligned}
L_{back}(H+z, \boldsymbol{\rho}, \mathbf{s}, t) &= A_t \frac{R_t}{\pi} \delta(\boldsymbol{\rho} - \boldsymbol{\rho}_t) \frac{Q T_a T_{aw}}{(2\pi)^2} \int \dots \int \Psi_{TX}(\boldsymbol{\kappa}) \Theta_{TX}(\boldsymbol{\kappa}(H+z/m)) \\
&\cdot K(z, \boldsymbol{\kappa}, \mathbf{0}, \tau) \exp(-j\boldsymbol{\kappa} \cdot \boldsymbol{\rho}) \exp(j\boldsymbol{\kappa} \cdot (\boldsymbol{\rho}_{TX} + (H+z/m)\mathbf{s}_{TX})) d\boldsymbol{\kappa}. \tag{20}
\end{aligned}$$

For a diffuse source on the target surface radiating upwards, the radiance is given by (10). The radiance presented to the receiver is given by (11) where $L_{back}(H + z, \boldsymbol{\rho}, \mathbf{s}, t)$ is given by (20). Since two arbitrary functions $f(x)$ and $g(x)$ satisfy $f(x)\delta(x - x_0) * g(x) = f(x_0)g(x - x_0)$, the received radiance is

$$\begin{aligned}
L_{RX}(\boldsymbol{\rho}, \mathbf{s}, t) &= \frac{Q A_t T_a^2 T_{aw}^2 R_t}{m^2 \pi} \int \cdots \int \Psi_{TX}(\boldsymbol{\kappa}_1) \Theta_{TX}(\boldsymbol{\kappa}_1(H + z/m)) \\
&\cdot (K(z, \boldsymbol{\kappa}_1, \mathbf{0}, \tau) *_{\tau} K(z, \boldsymbol{\kappa}_2, -z\boldsymbol{\kappa}_2, \tau)) \exp(-j\boldsymbol{\kappa}_1 \cdot \boldsymbol{\rho}_t) \exp(j\boldsymbol{\kappa}_1 \cdot (\boldsymbol{\rho}_{TX} + (H + z/m)\mathbf{s}_{TX})) \\
&\cdot \exp(-j\boldsymbol{\kappa}_2 \cdot (\boldsymbol{\rho} - \boldsymbol{\rho}_t)) \exp(-j(H + z/m)\boldsymbol{\kappa}_2 \cdot \mathbf{s}) \frac{d\boldsymbol{\kappa}_1}{(2\pi)^2} \frac{d\boldsymbol{\kappa}_2}{(2\pi)^2}, \tag{21}
\end{aligned}$$

where $t = 2H/c + 2zm/c + \tau$. Incorporating the aperture function, reception pattern, receiver FOV and aperture area, we have the return from a target at depth z and location $\boldsymbol{\rho}_t$ as

$$P_t(t, \boldsymbol{\rho}_t) = A_{RX} \Omega_{RX} \int \cdots \int L_{RX}(\boldsymbol{\rho}, \mathbf{s}, t) \psi_{RX}(\boldsymbol{\rho} - \boldsymbol{\rho}_{RX}) \theta_{RX}(\mathbf{s} - \mathbf{s}_{RX}) d\boldsymbol{\rho} d\mathbf{s}. \tag{22}$$

Inserting $L_{RX}(\boldsymbol{\rho}, \mathbf{s}, t)$ from (21), we have

$$\begin{aligned}
P_t(t, \boldsymbol{\rho}_t) &= C_t \int \cdots \int \Psi_{TX}(\boldsymbol{\kappa}_1) \Theta_{TX}(\boldsymbol{\kappa}_1(H + z/m)) \Psi_{RX}^*(\boldsymbol{\kappa}_2) \Theta_{RX}^*(\boldsymbol{\kappa}_2(H + z/m)) \\
&\cdot (K(z, \boldsymbol{\kappa}_1, \mathbf{0}, \tau) *_{\tau} K(z, \boldsymbol{\kappa}_2, -z\boldsymbol{\kappa}_2, \tau)) \exp(j\boldsymbol{\kappa}_1 \cdot (\boldsymbol{\rho}_{TX} + (H + z/m)\mathbf{s}_{TX})) \\
&\cdot \exp(-j\boldsymbol{\rho}_t \cdot (\boldsymbol{\kappa}_1 - \boldsymbol{\kappa}_2)) \exp(-j\boldsymbol{\kappa}_2 \cdot (\boldsymbol{\rho}_{RX} + (H + z/m)\mathbf{s}_{RX})) \frac{d\boldsymbol{\kappa}_1}{(2\pi)^2} \frac{d\boldsymbol{\kappa}_2}{(2\pi)^2}, \tag{23}
\end{aligned}$$

where $C_t = QA_{RX}\Omega_{RX}A_tT_a^2T_{aw}^2R_t/(m^2\pi)$. In terms of lidar range,

$$\begin{aligned}
P_t(\zeta, \boldsymbol{\rho}_t) &= C_t \int \cdots \int \Psi_{TX}(\boldsymbol{\kappa}_1) \Theta_{TX}(\boldsymbol{\kappa}_1(H + D/m)) \Psi_{RX}^*(\boldsymbol{\kappa}_2) \Theta_{RX}^*(\boldsymbol{\kappa}_2(H + D/m)) \\
&\cdot (K(D, \boldsymbol{\kappa}_1, \mathbf{0}, \tau) *_{\tau} K(D, \boldsymbol{\kappa}_2, -D\boldsymbol{\kappa}_2, \tau)) \exp(j\boldsymbol{\kappa}_1 \cdot (\boldsymbol{\rho}_{TX} + (H + D/m)\mathbf{s}_{TX})) \\
&\cdot \exp(-j\boldsymbol{\rho}_t \cdot (\boldsymbol{\kappa}_1 - \boldsymbol{\kappa}_2)) \exp(-j\boldsymbol{\kappa}_2 \cdot (\boldsymbol{\rho}_{RX} + (H + D/m)\mathbf{s}_{RX})) \frac{d\boldsymbol{\kappa}_1}{(2\pi)^2} \frac{d\boldsymbol{\kappa}_2}{(2\pi)^2}, \tag{24}
\end{aligned}$$

where $\zeta = D + \frac{c\tau}{2m}$ and D is the target depth. For an arbitrary target with spatial extent $\psi_t(\boldsymbol{\rho})$, we have

$$P_{trgt}(\zeta, \boldsymbol{\rho}) = \iint P_t(\zeta, \boldsymbol{\rho}_t) \psi_t(\boldsymbol{\rho} - \boldsymbol{\rho}_t) d\boldsymbol{\rho}_t. \tag{25}$$

D. Shadowing

Due to the shadow behind the target there is a loss of radiance that would otherwise be collected by the receiver. This loss is a negative perturbation to the background water return in (18), since (18) includes backscattered photons from behind the target. Calculated similarly as the background water return, the loss term is

$$\begin{aligned}
P_s(\zeta, \boldsymbol{\rho}_t) = & C_s \int \cdots \int \Psi_{TX}(\boldsymbol{\kappa}_1) \Theta_{TX}(\boldsymbol{\kappa}_1(H + \zeta/m)) \Psi_{RX}^*(\boldsymbol{\kappa}_2) \Theta_{RX}^*(\boldsymbol{\kappa}_2(H + \zeta/m)) \\
& \cdot \exp(j\boldsymbol{\kappa}_1 \cdot (\boldsymbol{\rho}_{TX} + (H + \zeta/m)\mathbf{s}_{TX})) \exp(-j\boldsymbol{\kappa}_2 \cdot (\boldsymbol{\rho}_{RX} + (H + \zeta/m)\mathbf{s}_{RX})) \\
& \cdot \exp(-j\boldsymbol{\rho}_t \cdot (\boldsymbol{\kappa}_1 - \boldsymbol{\kappa}_2)) \frac{c}{2m} \int_0^{2(\zeta-D)m/c} (K(\zeta, \boldsymbol{\kappa}_1, \mathbf{0}, \tau) *_{\tau} K(\zeta, \boldsymbol{\kappa}_2, -\zeta\boldsymbol{\kappa}_2, \tau)) d\tau \frac{d\boldsymbol{\kappa}_1}{(2\pi)^2} \frac{d\boldsymbol{\kappa}_2}{(2\pi)^2},
\end{aligned} \tag{26}$$

where $C_s = QA_t A_{RX} \Omega_{RX} T_a^2 T_{aw}^2 \beta(\pi)/m^2$. Equation (26) is valid for $\zeta \geq D$. Similar to (25), the loss of radiance for an extended target is

$$P_{shdw}(\zeta, \boldsymbol{\rho}) = \iint P_s(\zeta, \boldsymbol{\rho}_t) \psi_t(\boldsymbol{\rho} - \boldsymbol{\rho}_t) d\boldsymbol{\rho}_t. \tag{27}$$

E. Total return

The total return at the receiver is the sum of the target return (25) and the background (water) return (18) from the water column, less the loss term (27). The bottom return (16) also can be included if the lidar range of interest contains the bottom, i.e. $\zeta \geq D$.

3. Evaluation of the integrals

To compute the bistatic lidar returns presented above, we insert the medium transfer function into the integrals and perform the integration over spatial frequency. The analytical model for the beam spread function is given by McLean et al.,²

$$\begin{aligned}
k(z, \boldsymbol{\rho}, \mathbf{s}, \tau) = & \delta(\boldsymbol{\rho}) \delta(\mathbf{s}) \delta(\tau) \exp(-(a + b)z) \\
& + (1 - \exp(-bz)) \exp(-a(z + c\tau/m)) g(z, \tau) h(z, \boldsymbol{\rho}, \mathbf{s}, \tau),
\end{aligned} \tag{28}$$

where the first term accounts for unscattered photons, that is, $\tau = 0$, and the second term is for photons that experience scattering, with $\tau > 0$. The term $(1 - \exp(-bz))$ is the probability that a photon will be scattered. Here a and b are the *absorption coefficient* and *scattering coefficient* of water, respectively. The distribution of the variable τ is dependent on depth and is given by

$$g(z, \tau) = \frac{\mu}{\sigma^2 \Gamma(\mu^2/\sigma^2)} \left(\frac{\mu\tau}{\sigma^2} \right)^{\mu^2/\sigma^2 - 1} \exp\left(-\frac{\mu\tau}{\sigma^2}\right), \quad (29)$$

which is a gamma distribution. Here, $\Gamma(\cdot)$ is the gamma function.¹² Note that the mean μ and the variance σ^2 of the distribution are dependent on depth, z . They can be evaluated using the statistical model due to Lutomirski et al.^{1,2,13} The distribution of τ being gamma is implied by the Poisson nature of the photon scattering. As a photon undergoes multiple scattering, the time interval between scattering events can be modeled as an exponential random variable, because the arrival time of a photon to a scatterer is a Poisson random variable, and from the photon's point of view, the "arrival" of a scatterer is Poisson. The multipath time τ is the sum of the time intervals between scattering events. Since the sum of exponential random variables is a gamma random variable, τ has a gamma distribution.

From (28), we have the beam transfer function

$$\begin{aligned} K(z, \boldsymbol{\kappa}, \mathbf{q}, \tau) &= \delta(\tau) \exp(-(a+b)z) \\ &+ (1 - \exp(-bz)) \exp(-a(z + c\tau/m)) g(z, \tau) H(z, \boldsymbol{\kappa}, \mathbf{q}, \tau). \end{aligned} \quad (30)$$

By using the time-independent solution for the beam transfer function with small-angle scattering, and assuming that all photons in the beam scatter, $H(z, \boldsymbol{\kappa}, \mathbf{q}, \tau)$ is calculated as,^{1,2}

$$H(z, \boldsymbol{\kappa}, \mathbf{q}, \tau) = \exp\left(-\frac{\tau c}{mz} \left(q^2 + z\mathbf{q} \cdot \boldsymbol{\kappa} + \frac{1}{3}\kappa^2 z^2\right)\right), \quad (31)$$

where $\kappa = |\boldsymbol{\kappa}|$ and $q = |\mathbf{q}|$. Note that

$$H(z, \boldsymbol{\kappa}, \mathbf{0}, \tau) = H(z, \boldsymbol{\kappa}, -z\boldsymbol{\kappa}, \tau). \quad (32)$$

Then, for the temporal convolution expression, we have

$$\begin{aligned}
K(z, \boldsymbol{\kappa}_1, \mathbf{0}, \tau) *_{\tau} K(z, \boldsymbol{\kappa}_2, -z\boldsymbol{\kappa}_2, \tau) &= \exp(-2az) [\delta(\tau) \exp(-2bz) \\
&+ \exp(-bz) (1 - \exp(-bz)) \exp(-ac\tau/m) g(z, \tau) (H(z, \boldsymbol{\kappa}_1, \mathbf{0}, \tau) + H(z, \boldsymbol{\kappa}_2, -z\boldsymbol{\kappa}_2, \tau)) \\
&+ (1 - \exp(-bz))^2 \exp(-ac\tau/m) (g(z, \tau)H(z, \boldsymbol{\kappa}_1, \mathbf{0}, \tau) *_{\tau} g(z, \tau)H(z, \boldsymbol{\kappa}_2, -z\boldsymbol{\kappa}_2, \tau))]. \quad (33)
\end{aligned}$$

We assume that the radiation and reception patterns are Gaussian functions, that is,

$$\theta_i(\mathbf{s}) = \frac{1}{\pi\theta_{i,x}\theta_{i,y}} \exp\left(-s_x^2/\theta_{i,x} - s_y^2/\theta_{i,y}^2\right), \quad (34)$$

where i is either TX or RX, denoting transmitter or receiver. The subscripts x and y denote the x and y components of the vector. A Gaussian pattern is in agreement with the spatially Gaussian shape of the laser beam.¹⁴ Correspondingly, in the Fourier transform domain

$$\Theta_i(\mathbf{q}) = \exp\left(-\frac{1}{4}(q_x^2\theta_{i,x}^2 + q_y^2\theta_{i,y}^2)\right). \quad (35)$$

The transmitter and receiver FOV are given as $\Omega_i = \pi\theta_{i,x}\theta_{i,y}$. Also, we assume $\psi_{TX}(\boldsymbol{\rho}) = \delta(\boldsymbol{\rho})$. The radiance field changes slowly across the receiver aperture. We, therefore, assume $\psi_{RX}(\boldsymbol{\rho}) = \delta(\boldsymbol{\rho})$. For the Fourier transform of the aperture functions, we have $\Psi_i(\boldsymbol{\kappa}) = 1$, where, again, i denotes either TX or RX. In practice, this is true for a PMT. The aperture of a CCD receiver is too large for this to be accurate. However, each element of the CCD array can be treated as a separate receiver with a much narrower receiver FOV.

A. Water return

Inserting Equations (33) and (35) and the Fourier transforms of $\psi_{TX}(\boldsymbol{\rho})$ and $\psi_{RX}(\boldsymbol{\rho})$ into (18), we have the background water return expressed as

$$\begin{aligned}
P_w(\zeta) = C_w \int_{L_1}^{L_2} \frac{c}{2m} \exp(-2a\zeta) & \left[\delta(\tau) \exp(-2b\zeta) \underbrace{\iint \exp(-X_1 + j\boldsymbol{\kappa} \cdot \mathbf{X}_2) \frac{d\boldsymbol{\kappa}}{(2\pi)^2}}_{I_1(\zeta)} \right. \\
& + 2 \exp(-b\zeta) (1 - \exp(-b\zeta)) \exp(-ac\tau/m) g(\zeta, \tau) \\
& \cdot \underbrace{\iint \exp(-X_1 + j\boldsymbol{\kappa} \cdot \mathbf{X}_2) H(\zeta, \boldsymbol{\kappa}, \mathbf{0}, \tau) \frac{d\boldsymbol{\kappa}}{(2\pi)^2}}_{I_2(\zeta)} \\
& + (1 - \exp(-b\zeta))^2 \exp(-ac\tau/m) \\
& \left. \cdot \underbrace{\iint \exp(-X_1 + j\boldsymbol{\kappa} \cdot \mathbf{X}_2) (g(\zeta, \tau)H(\zeta, \boldsymbol{\kappa}, \mathbf{0}, \tau) *_{\tau} g(\zeta, \tau)H(\zeta, \boldsymbol{\kappa}, -\zeta\boldsymbol{\kappa}, \tau)) \frac{d\boldsymbol{\kappa}}{(2\pi)^2}}_{I_3(\zeta)} d\tau, \right. \quad (36)
\end{aligned}$$

where $L_1 = 0$, $L_2 = 2\zeta m/c$ for $\zeta < D$ and $L_1 = 2(\zeta - D)m/c$, $L_2 = 2\zeta m/c$ for $\zeta \geq D$, with D being the bottom depth. In writing (36), we used (32). The shorthand notation X_1 is defined as

$$X_1 = \frac{1}{4} (H + \zeta/m)^2 \left(\kappa_x^2 (\theta_{RX,x}^2 + \theta_{TX,x}^2) + \kappa_y^2 (\theta_{RX,y}^2 + \theta_{TX,y}^2) \right) \quad (37)$$

where the subscripts x and y stand for the x and y components of the vector. Also, we have

$$\mathbf{X}_2 = (\boldsymbol{\rho}_{TX} - \boldsymbol{\rho}_{RX}) + (H + \zeta/m)(\mathbf{s}_{TX} - \mathbf{s}_{RX}). \quad (38)$$

The x and y components are

$$X_{2,i} = (\rho_{TX,i} - \rho_{RX,i}) + (H + \zeta/m)(s_{TX,i} - s_{RX,i}), \quad (39)$$

where i is either x or y .

The task of calculating the water return (18) has been reduced to calculating the integrals $I_1(\zeta)$, $I_2(\zeta)$, and $I_3(\zeta)$ in (36). The outer integral over τ is computed numerically. Integral I_2 can be evaluated explicitly using the Fourier transform identity

$$\frac{1}{2\pi} \int \exp(-ax^2) \exp(jbx) dx = \frac{1}{2\sqrt{\pi a}} \exp(-b^2/4a) . \quad (40)$$

We insert

$$H(\zeta, \boldsymbol{\kappa}, \mathbf{0}, \tau) = \exp\left(-\frac{1}{3m}\zeta\tau c\kappa^2\right), \quad (41)$$

where $\kappa^2 = |\boldsymbol{\kappa}|^2 = (\kappa_x^2 + \kappa_y^2)$, into the integral I_2 and use (40). This yields

$$\begin{aligned} I_2(\zeta) &= \left(\pi(H + \zeta/m)^2 \left(\theta_{RX,x}^2 + \theta_{TX,x}^2 + \frac{4\zeta\tau c}{3m(H + \zeta/m)^2} \right)^{\frac{1}{2}} \right. \\ &\quad \cdot \left. \left(\theta_{RX,y}^2 + \theta_{TX,y}^2 + \frac{4\zeta\tau c}{3m(H + \zeta/m)^2} \right)^{\frac{1}{2}} \right)^{-1} \\ &\quad \cdot \exp\left(-\frac{((\rho_{TX,x} - \rho_{RX,x}) + (H + \zeta/m)(s_{TX,x} - s_{RX,x}))^2}{(H + \zeta/m)^2(\theta_{RX,x}^2 + \theta_{TX,x}^2) + \frac{4\zeta\tau c}{3m}}}\right) \\ &\quad \cdot \exp\left(-\frac{((\rho_{TX,y} - \rho_{RX,y}) + (H + \zeta/m)(s_{TX,y} - s_{RX,y}))^2}{(H + \zeta/m)^2(\theta_{RX,y}^2 + \theta_{TX,y}^2) + \frac{4\zeta\tau c}{3m}}}\right). \end{aligned} \quad (42)$$

Furthermore, $I_1(\zeta) = I_2(\zeta)|_{\tau=0}$. In $I_3(\zeta)$, we have

$$\begin{aligned} g(z, \tau)H(z, \boldsymbol{\kappa}, \mathbf{0}, \tau) *_{\tau} g(z, \tau)H(z, \boldsymbol{\kappa}, -z\boldsymbol{\kappa}, \tau) &= \\ \int g(\zeta, \tau') H(\zeta, \boldsymbol{\kappa}, \mathbf{0}, \tau') H(\zeta, \boldsymbol{\kappa}, -z\boldsymbol{\kappa}, \tau - \tau') g(\zeta, \tau - \tau') d\tau', \end{aligned} \quad (43)$$

where

$$\begin{aligned} H(\zeta, \boldsymbol{\kappa}, \mathbf{0}, \tau')H(\zeta, \boldsymbol{\kappa}, -z\boldsymbol{\kappa}, \tau - \tau') &= \exp\left(-\frac{1}{3m}\zeta\tau'c\kappa^2\right) \exp\left(-\frac{1}{3m}\zeta(\tau - \tau')c\kappa^2\right) \\ &= \exp\left(-\frac{1}{3m}\zeta\tau c\kappa^2\right) \\ &= H(\zeta, \boldsymbol{\kappa}, \mathbf{0}, \tau). \end{aligned} \quad (44)$$

Now the integral I_3 resembles the integral I_2 except for the autoconvolution of $g(\zeta, \tau)$. Thus, we have

$$I_3(\zeta) = (g(\zeta, \tau) *_{\tau} g(\zeta, \tau)) I_2(\zeta), \quad (45)$$

where

$$g(\zeta, \tau) *_{\tau} g(\zeta, \tau) = \frac{\mu}{\sigma^2 \Gamma(2\mu^2/\sigma^2)} \left(\frac{\mu\tau}{\sigma^2}\right)^{2\mu^2/\sigma^2-1} \exp\left(-\frac{\mu\tau}{\sigma^2}\right), \quad (46)$$

for $\tau \geq 0$, which is calculated by using the characteristic function of the gamma distribution.

B. Bottom return

The bottom return contains the integrals I_1 , I_2 , and I_3 , but does not contain the integral over τ .

Thus, for the bottom return, we have

$$P_b(\zeta) = C_b \exp(-2aD) [\delta(\tau) \exp(-2bD) I_1(D) + 2 \exp(-bD) (1 - \exp(-bD)) \cdot \exp(-ac\tau/m) g(D, \tau) I_2(D) + (1 - \exp(-bD))^2 \exp(-ac\tau/m) I_3(D)], \quad (47)$$

where $\zeta = D + c\tau/2m$ and D is the bottom depth.

C. Shadowing

Inserting the aperture functions, radiation/reception patterns and the temporal convolution expression for the medium transfer function into (26), the loss of radiance due to shadowing is given as

$$P_s(\zeta, \boldsymbol{\rho}_t) = C_s \int_0^{2(\zeta-D)m/c} \frac{c}{2m} \exp(-2a\zeta) \left[\delta(\tau) \exp(-2b\zeta) \underbrace{\iint \exp(-Y_1 + jY_3) \frac{d\boldsymbol{\kappa}_1}{(2\pi)^2}}_{J_1(\zeta)} \cdot \underbrace{\iint \exp(-Y_2 + jY_4) \frac{d\boldsymbol{\kappa}_2}{(2\pi)^2}}_{J_2(\zeta)} + \exp(-b\zeta) (1 - \exp(-b\zeta)) \exp(-ac\tau/m) g(\zeta, \tau) J_1(\zeta) \cdot \underbrace{\iint \exp(-Y_2 + jY_4) H(\zeta, \boldsymbol{\kappa}_2, -\zeta\boldsymbol{\kappa}_2, \tau) \frac{d\boldsymbol{\kappa}_2}{(2\pi)^2}}_{J_3(\zeta)} + \exp(-b\zeta) (1 - \exp(-b\zeta)) \exp(-ac\tau/m) \cdot g(\zeta, \tau) J_2(\zeta) \underbrace{\iint \exp(-Y_1 + jY_3) H(\zeta, \boldsymbol{\kappa}_1, \mathbf{0}, \tau) \frac{d\boldsymbol{\kappa}_1}{(2\pi)^2}}_{J_4(\zeta)} + (1 - \exp(-b\zeta))^2 \cdot \exp(-ac\tau/m) \underbrace{\int \dots \int \exp(-Y_1 - Y_2 + jY_3 + jY_4) p(\zeta, \boldsymbol{\kappa}_1, \boldsymbol{\kappa}_2, \tau) \frac{d\boldsymbol{\kappa}_1}{(2\pi)^2} \frac{d\boldsymbol{\kappa}_2}{(2\pi)^2}}_{J_5(\zeta)} d\tau. \quad (48)$$

where

$$\begin{aligned}
Y_1 &= \frac{1}{4}(H + \zeta/m)^2 \left(\kappa_{1,x}^2 \theta_{TX,x}^2 + \kappa_{1,y}^2 \theta_{TX,y}^2 \right) \\
Y_2 &= \frac{1}{4}(H + \zeta/m)^2 \left(\kappa_{2,x}^2 \theta_{RX,x}^2 + \kappa_{2,y}^2 \theta_{RX,y}^2 \right) \\
Y_3 &= \kappa_{1,x} (\rho_{TX,x} + (H + \zeta/m) s_{TX,x} - \rho_{t,x}) \\
&\quad + \kappa_{1,y} (\rho_{TX,y} + (H + \zeta/m) s_{TX,y} - \rho_{t,y}) \\
Y_4 &= -\kappa_{2,x} (\rho_{RX,x} + (H + \zeta/m) s_{RX,x} - \rho_{t,x}) \\
&\quad - \kappa_{2,y} (\rho_{RX,y} + (H + \zeta/m) s_{RX,y} - \rho_{t,y}).
\end{aligned} \tag{49}$$

and

$$p(\zeta, \boldsymbol{\kappa}_1, \boldsymbol{\kappa}_2, \tau) = g(\zeta, \tau) H(\zeta, \boldsymbol{\kappa}_1, \mathbf{0}, \tau) *_{\tau} g(\zeta, \tau) H(\zeta, \boldsymbol{\kappa}_2, -\zeta \boldsymbol{\kappa}_2, \tau). \tag{50}$$

For the evaluation of J_1 , we insert Y_1 and Y_3 from (49) and use (40), which yields

$$\begin{aligned}
J_1(\zeta) &= \left(\pi(H + \zeta/m)^2 \theta_{TX,x} \theta_{TX,y} \right)^{-1} \\
&\quad \cdot \exp \left(-\frac{(\rho_{TX,x} + (H + \zeta/m) s_{TX,x} - \rho_{t,x})^2}{(H + \zeta/m)^2 \theta_{TX,x}^2} \right) \\
&\quad \cdot \exp \left(-\frac{(\rho_{TX,y} + (H + \zeta/m) s_{TX,y} - \rho_{t,y})^2}{(H + \zeta/m)^2 \theta_{TX,y}^2} \right).
\end{aligned} \tag{51}$$

The integral $J_2(\zeta)$ is the same as $J_1(\zeta)$ except that the subscript TX is replaced by RX. The calculation of $J_3(\zeta)$ is performed similarly after recalling (32) and inserting (41) into the integral

J_3 . We obtain

$$\begin{aligned}
J_3(\zeta) &= \left(\pi(H + \zeta/m)^2 \left(\theta_{RX,x}^2 + \frac{4\zeta\tau c}{3m(H + \zeta/m)^2} \right)^{\frac{1}{2}} \right. \\
&\quad \left. \cdot \left(\theta_{RX,y}^2 + \frac{4\zeta\tau c}{3m(H + \zeta/m)^2} \right)^{\frac{1}{2}} \right)^{-1} \\
&\quad \cdot \exp \left(-\frac{(\rho_{RX,x} + (H + \zeta/m) s_{RX,x} - \rho_{t,x})^2}{(H + \zeta/m)^2 \theta_{RX,x}^2 + \frac{4\zeta\tau c}{3m}} \right) \\
&\quad \cdot \exp \left(-\frac{(\rho_{RX,y} + (H + \zeta/m) s_{RX,y} - \rho_{t,y})^2}{(H + \zeta/m)^2 \theta_{RX,y}^2 + \frac{4\zeta\tau c}{3m}} \right).
\end{aligned} \tag{52}$$

The integral $J_4(\zeta)$ is the same as $J_3(\zeta)$ except that the subscript RX is replaced by TX.

Evaluation of $J_5(\zeta)$ requires calculation of $p(\zeta, \kappa_1, \kappa_2, \tau)$, given by (50). We can express each of the terms in the convolution as a gamma distribution to within a scale factor. Let the corresponding random variables be represented by γ_1 and γ_2 , respectively. Since $p(\zeta, \kappa_1, \kappa_2, \tau)$ is a convolution of two gamma distributions corresponding to random variables γ_1 and γ_2 , it is a gamma distribution itself, let us say, for random variable γ_3 , where $\gamma_3 = \gamma_1 + \gamma_2$. Assuming γ_1 and γ_2 are independent, and calculating the mean and variance of γ_3 , we obtain,

$$p(\zeta, \kappa_1, \kappa_2, \tau) = \frac{c_0^{2x}}{c_1^x c_2^x} \left(\frac{c_3^y}{\Gamma(y)} \tau^{y-1} \exp(-c_3 \tau) \right) \quad (53)$$

for $\tau > 0$, where $x = \mu^2/\sigma^2$, $c_0 = \mu/\sigma^2$, $Z_1 = c\kappa_1^2\zeta/3m$, $Z_2 = c\kappa_2^2\zeta/3m$, $c_1 = c_0 + Z_1$, $c_2 = c_0 + Z_2$, $c_3 = c_1 c_2 (c_1 + c_2) / (c_1^2 + c_2^2)$, $y = x(c_1 + c_2)^2 / (c_1^2 + c_2^2)$, with μ and σ^2 the mean and variance of the gamma distribution with parameters x and c_0 . The resulting expression for J_5 is difficult to integrate over κ_1 or κ_2 . We, however, can approximate it roughly as

$$p(\zeta, \kappa_1, \kappa_2, \tau) \approx (g(\zeta, \tau) *_{\tau} g(\zeta, \tau)) \exp(-\tau Z_1) \exp(-\tau Z_2). \quad (54)$$

This is exact when $\kappa_1 = \kappa_2 = 0$ and is a good approximation when κ_1 and κ_2 are large. Also, note that the contribution of J_5 is small with respect to the other components of the expression (48) when the scattering coefficient b is small. Using the approximation, we obtain

$$J_5(\zeta) = (g(\zeta, \tau) *_{\tau} g(\zeta, \tau)) J_3(\zeta) J_4(\zeta). \quad (55)$$

This completes the calculation of (26).

D. Target return

The target return in (24) is evaluated as

$$\begin{aligned}
P_t(\zeta, \boldsymbol{\rho}_t) = & C_t \exp(-2aD) [\delta(\tau) \exp(-2bD) J_1(D)J_2(D) \\
& + \exp(-bD) (1 - \exp(-bD)) \exp(-ac\tau/m) g(D, \tau)J_1(D)J_3(D) \\
& + \exp(-bD) (1 - \exp(-bD)) \exp(-ac\tau/m) g(D, \tau)J_2(D)J_4(D) \\
& + (1 - \exp(-bD))^2 \exp(-ac\tau/m) J_5(D)], \tag{56}
\end{aligned}$$

where D is the target depth.

E. Total return

The lidar return from the bottom, the water medium and a submerged target in terms of the lidar range are given by (16), (18) and (24). The loss of radiance due to shadowing behind the target is given by (26). Using a statistical model for the beam spread function together with reasonable aperture functions and radiation and reception patterns for the transmitter and receiver, we express the equations as (36), (47), (48), and (56). The integrals over the spatial frequency variable in these expressions are evaluated analytically. The integrals over the variable τ are to be computed numerically.

4. Synthetic returns from a CCD array

Synthetic lidar returns can be generated using the bistatic lidar equations derived in the previous sections. Using these equations we can compute the background return for a variety of water types, the return from the bottom of the water column (e.g. the ocean floor) and the target return from a submerged object. Our analysis assumes a flat ocean surface, which is practical for the return from a calm ocean environment. Surface effects also can be incorporated into the lidar return model.^{10,15}

For the CCD return, we assume that each pixel is a separate receiver element and we assign

different receiver position and direction offsets, and perform the bistatic lidar computations. We account for the pulse shape by convolving the return with the temporal pulse shape of the laser. We also account for the camera integration time, over the camera gate, at each CCD element. In our simulations, we assumed a 32×32 CCD array, with the transmitter position coinciding with the center of the CCD and a corresponding position offset assigned to each CCD element. Given the size of the footprint of the transmitted beam on the surface of the water, which can be calculated using the transmitter FOV, we divided the footprint into smaller patches, each of which was a smaller “pixel footprint” on the water surface, corresponding to one of the CCD elements. The size and location of a pixel footprint provided the FOV and direction offset for its corresponding CCD element.

An example of a synthetic CCD return is shown in Figure 2. The corresponding CCD return from a real ocean lidar data set is shown in Figure 3. The real data set is from a previous study (1998 Competitive Evaluation Field Test (CEFT), Panama City, FL) which was produced by an airborne lidar imaging system designed by Lockheed Sanders Corp. for the U. S. Navy. The object was a sphere of 1 m diameter, at a 6.4 m (21 ft) depth. The altitude of the airborne lidar system was 360 m. The object was simulated as a flat diffuse circular surface of 1 m diameter, which corresponds to the upper hemisphere of the true (spherical) object. A more elaborate simulation of the object would use concentric rings of flat diffuse surfaces placed deeper with increasing radius. Use of a flat diffuse surface is appropriate for simulation of opaque objects illuminated by an airborne lidar system from large elevation angles (small θ angle). Note that, in general, it is possible to simulate accurately an object of complicated shape by using (25), at the expense of computation.

The water parameters such as absorption, scattering and backscattering coefficients were chosen from a table given by Mobley⁹ for coastal ocean ($a = 0.179$, $b = 0.219$, $b_b = 0.0285$), which are tabulated also by Walker and McLean.¹ The wavelength of the laser was 532 nm. The diameter of

the beam footprint on the ocean surface was approximately 12 m. The in-water angle θ_2 in Figure 1 was about 8° .

Note that the simulated return does not account for noise. By adding Gaussian noise at 20 dB SNR to the synthetic return in Figure 2, we produced the result in Figure 4. The real ocean data shown in Figure 3 contains the effect of waves on the ocean surface, which cause blurring.¹⁵ The Gaussian noise added to the synthetic return models the thermal noise well, but is not a good model for the effect of surface waves. An accurate simulation for the surface wave effect would use blurring filters of Gaussian shape.¹⁵ The shape parameters of the filters can be calculated from the height and slope statistics of surface waves.¹⁰

The synthetic lidar return appears to match the qualitative characteristics of the real data very well. Note the Gaussian structure of the base of the mesh surfaces. This is due to the spatially Gaussian shape of the laser beam.¹⁴

5. Conclusion

We have generalized the Walker-McLean lidar equations to the case of bistatic geometry. We have evaluated the resulting equations through a combination of analysis and numerical integration to generate synthetic CCD data. The synthetic data matched the characteristics of real ocean data quite well. Our data generation capability will facilitate algorithm development for airborne lidar imaging without the high cost of real data collection using an actual airborne lidar system.

Acknowledgments

This research was supported by the Office of Naval Research under grant N61331-00-1-G001.

References

1. Ronald E. Walker and John W. McLean, "Lidar equations for turbid media with pulse stretching," *Appl. Opt.* **38**, 2384–2397 (1999).
2. John W. McLean, Jonathan D. Freeman, and Ronald E. Walker, "Beam spread function with time dispersion," *Appl. Opt.* **37**, 4701–4711 (1998).
3. Iosif L. Katsev, Eleonora P. Zege, Alexander S. Prikhach, and Igor N. Polonsky, "Efficient technique to determine backscattered light power for various atmospheric and oceanic sounding and imaging systems," *J. Opt. Soc. Am. A* **14**, 1338–1346 (1997).
4. N. G. Jerlov, *Marine Optics*, (Elsevier Scientific Publishing, Amsterdam, 1976).
5. Akira Ishimaru, *Wave Propagation and Scattering in Random Media*, (Academic Press, New York, 1978).
6. Raymond M. Measures, *Laser Remote Sensing: Fundamentals and Applications*, (John Wiley & Sons, New York, 1984).
7. Leung Tsang, Jin Au Kong, and Robert T. Shin, *Theory of Microwave Remote Sensing*, (John Wiley & Sons, New York, 1985).
8. John R. Apel, *Principle of Ocean Physics*, (Academic Press, Orlando, FL, 1987).
9. Curtis D. Mobley, *Light and Water: Radiative Transfer in Natural Waters*, (Academic Press, San Diego, CA, 1994).

10. Ronald E. Walker, *Marine Light Field Statistics*, (John Wiley & Sons, New York, 1994).
11. Nail Çadallı, *Signal Processing Issues in Reflection Tomography*, PhD thesis, University of Illinois at Urbana-Champaign, (2001).
12. Athanasios Papoulis, *Probability, Random Variables and Stochastic Processes*, 3rd edition, (McGraw-Hill, New York, 1991).
13. R. F. Lutomirski, A. P. Ciervo, and G. J. Hall, “Moments of multiple scattering,” *Appl. Opt.* **34**, 7125–7136 (1995).
14. Bahaa E. A. Saleh and Malvin Carl Teich, *Fundamentals of Photonics*, (Wiley, New York, 1991).
15. John W. McLean and Jonathan D. Freeman, “Effects of ocean waves on airborne lidar imaging,” *Appl. Opt.* **35**, 3261–3269 (1996).

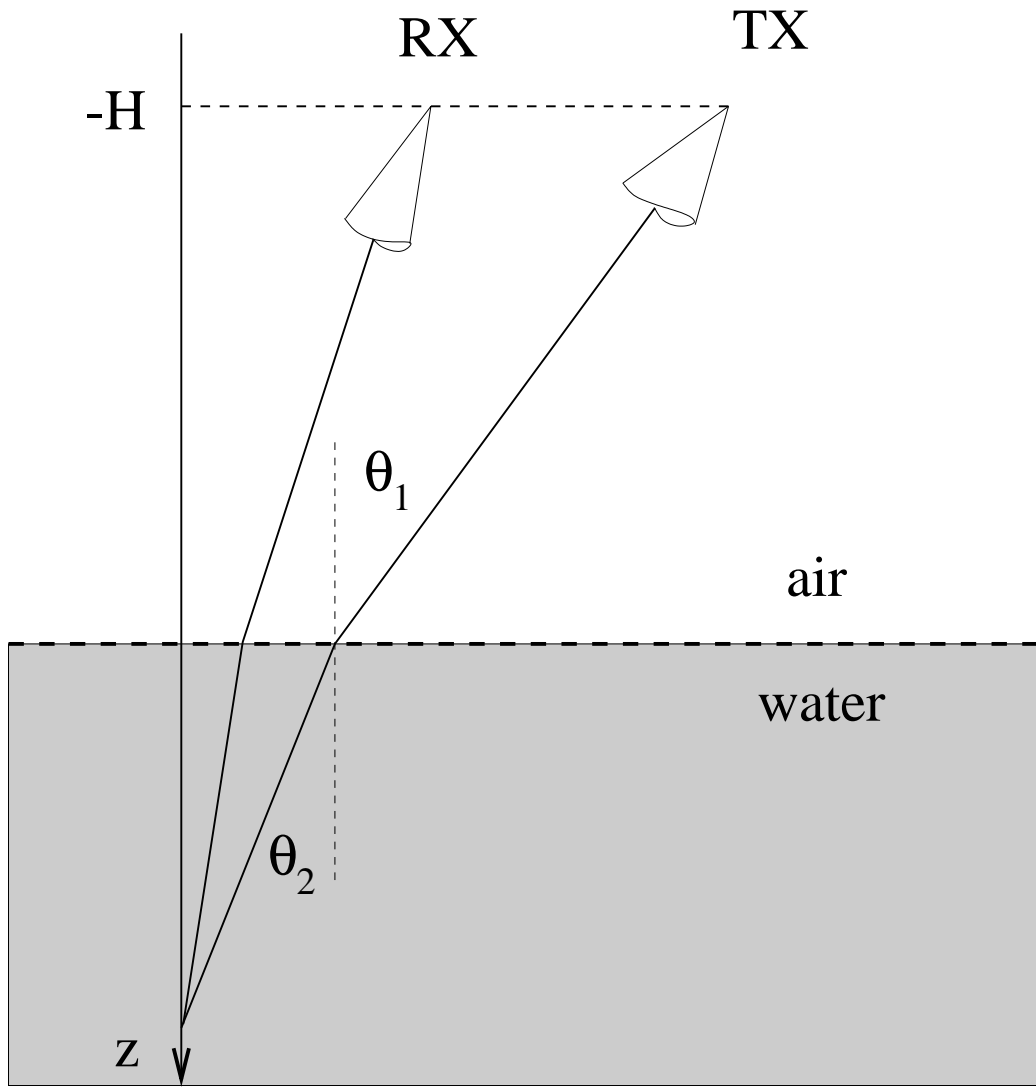


Figure 1, Çadallı et al., Appl. Opt.

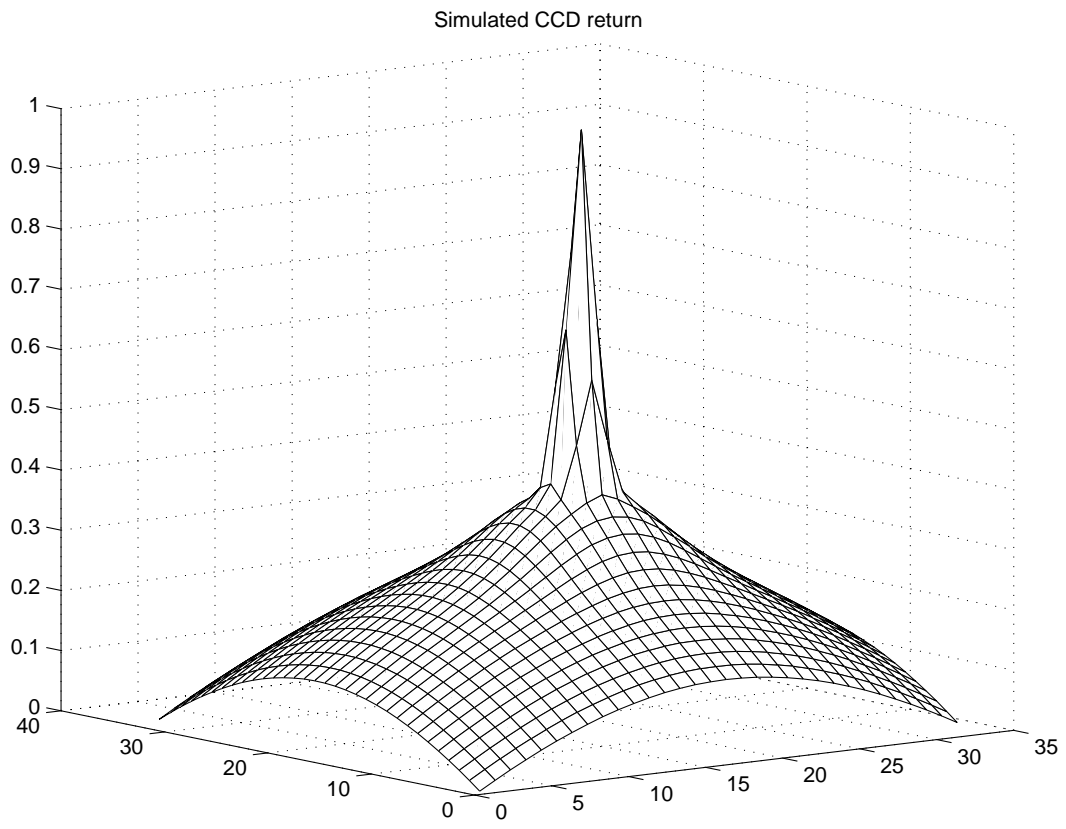


Figure 2, Çadallı et al., Appl. Opt.

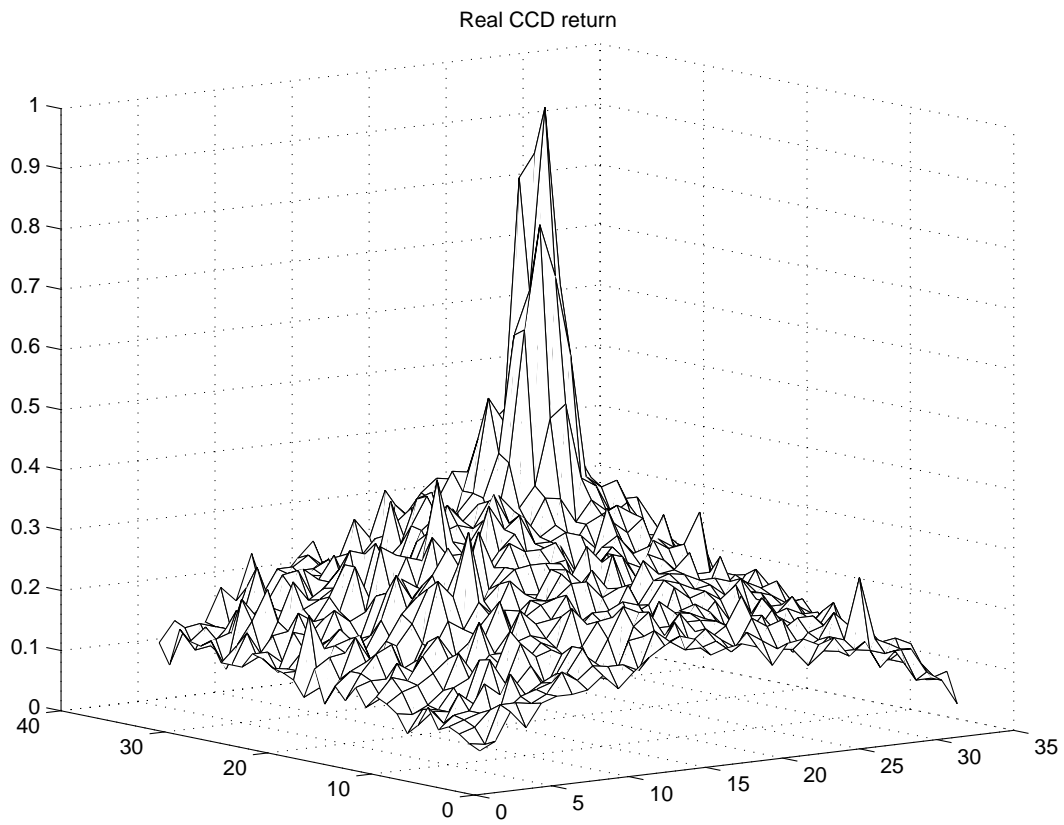


Figure 3, Çadallı et al., Appl. Opt.

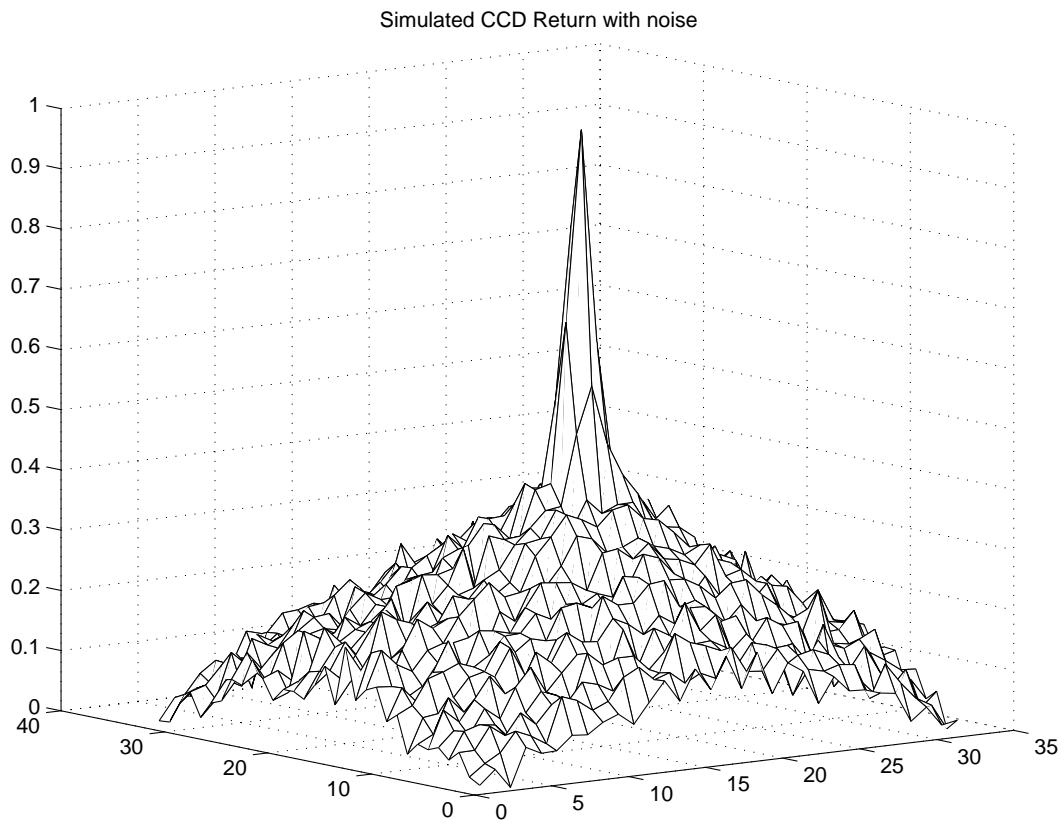


Figure 4, Çadallı et al., Appl. Opt.

Fig. 1. Bistatic lidar geometry.

Fig. 2. Simulated CCD return.

Fig. 3. Real CCD return from CEFT data.

Fig. 4. Simulated CCD return with noise.